Estimation of stiffness coefficients of an orthorhombic physical model from group velocity measurements

Faranak Mahmoudian, Gary Margrave, P.F. Daley, and Joe Wong

ABSTRACT

Physical model data have been used for many years to simulate exploration targets, as in the example of a fractured medium. Yet, physical modeling is challenging for at least two reasons; (1) the initial characterization of the medium is difficult, and (2) the large highly-directional transducers used as sources and receivers cause distortions. We present a straightforward method to characterize a physical model, composed of phenolic material, by employing the highly accurate group velocity measurements in estimating the orthorhombic stiffness coefficients of the medium. The large physical model transducers effect is discussed in another paper in this year's report. We measured the qP, qS$_V$, and qS$_H$ wave mode group velocities from direct-arrival traveltimes on physically modeled 3C transmission gathers. An approximate orthorhombic group velocity expression is used to estimate the off-diagonal stiffness coefficients. We show that estimates of the stiffness coefficients are consistent with measured velocity data. Theoretically predicted group velocities from the estimated stiffness coefficients are very close to the measured velocities. The stiffness coefficients values suggest that the experimental physical layer approximates a weakly anisotropic HTI layer. Hence our model simulates a vertically fractured transversely isotropic layer for physical modeling of fractured reservoir characterization, and for testing new anisotropic seismic data processing algorithms.

INTRODUCTION

Physical seismic modeling, an alternative to numerical modeling, provides valuable insights into wave propagation phenomena, and is a helpful tool in testing seismic processing algorithms. In physical modeling the seismic wave propagation and recordings are performed on small, laboratory-size geological models. Physical modeling has gained interest in studying fractured anisotropic media, as the real wave propagation is obtained without employing a non-ideal mathematical formulation (e.g., acoustic or elastic), or the computational challenges (e.g., grid dispersion) of numerical methods.

A principal requirement in physical modeling is the initial elastic characterization of the laboratory-size geological model. The symmetric 6×6 elastic stiffness matrix (C_{ij}), together with density (ρ), define an elastic anisotropic medium. For a vertically fractured medium, assuming orthorhombic symmetry, nine independent stiffness coefficients are required. The stiffness coefficients of a material are estimated from body-wave velocities in various directions. Generally, the available explicit expressions (e.g., Backus, 1965; Tsvankin, 2001) for phase velocity, in terms of stiffness coefficients, facilitate the estimations. The measurements of phase velocity, however, are inexact and cumbersome (Mah and Schmitt, 2001a).

For small specimens, the phase velocity measurements are obtained from ultrasonic transmission experiments that utilize relatively large transducers. When the transducers

are large compared to their separation, they will approximately transmit and receive plane waves over a large spatial interval (Figure 1). In that case, the measured transmission traveltimes will yield phase velocities (Dellinger and Vernik, 1994; Vestrum, 1994). Accommodating the direct measurement, the specimen gets appropriate cuts along various directions to make the desire contact plane for the flat-faced large transducers. When the transducers are small, the measured traveltimes yield group velocities. For larger physical models, therefore, the direct measurements of phase velocity are not possible. The phase velocities, however, can be determined using the (τ, p) transform on physically modeled transmission gathers (Kebaili and Schmitt, 1997; Mah and Schmitt, 2001a; van der Baan, 2002). This method implicitly assumes that the traveltimes themselves will yield group velocities.

In a standard physical modeling setting, with transducer size much smaller than the model dimensions, the transmitted traveltimes result in the direct measurements of group velocities. Every and Sachse (1992), Vestrum (1994), and Kim et al. (1995) employed group velocity measurements, using phase/group velocity relations converted them to phase velocities. With some optimization methods, they estimated the stiffness coefficients of an orthorhombic specimen.

There are no exact explicit expressions, except for orthorhombic symmetry axes, of the group velocity in terms of stiffness coefficients. Song and Every (2000), and Daley and Krebes (2006) introduced approximate expressions for group velocity as a function of orthorhombic stiffness coefficients. We use their explicit linearized qP group velocity formula to estimate the stiffness coefficients of an orthorhombic laminate phenolic layer, simulating a fractured medium, from the easy-to-measure direct group velocity measurements. Our group velocity measurements are obtained from physical model transmission data acquired over a simulated fractured layer at the CREWES project, University of Calgary, physical modeling lab. We estimate the diagonal stiffness coefficients from measurements along orthorhombic symmetry axes, and the off-diagonal ones from a least-squares inversion of quasi-P (qP) group velocity in various directions.

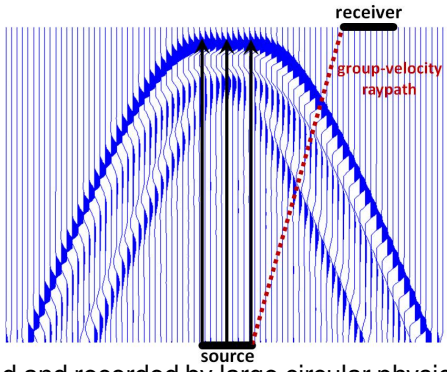

FIG. 1. The wavefront radiated and recorded by large circular physical model transducers, modeled by an acoustic finite-difference method. The black parallel vectors show the travel of the plane-wave portion of the wavefront. The transducer's size is chosen to be half of the layer thickness to exaggerate the plane-wave generation. The group velocity ray direction, edge-to-edge raypath, is that of the first arrival energy.

THEORY

In anisotropic media, velocities vary with the propagation direction. The phase velocity is velocity of seismic wave propagation in the direction of the wavefront normal, and the group (ray) velocity is velocity of energy propagation along a raypath from source to receiver. In an orthorhombic media the group and phase velocity, in various directions, are different except along the symmetry axes.

Consider the reference Cartesian coordinate system, (x_1, x_2, x_3), associated with the orthorhombic symmetry planes. In this reference coordinate system, the nine independent orthorhombic stiffness coefficients, are the six diagonal (C_{ii}) plus three off-diagonal (C_{23}, C_{13}, C_{12}). Throughout this paper we will deal exclusively with the density-normalized stiffness coefficients, $A_{ij} = C_{ij}/\rho$, which have the dimensions of velocity squared. The body-wave velocities along the principal axes determine diagonal stiffness coefficients (Table 1); three quasi-P (qP) velocities specify the $A_{ii}(i = 1 : 3)$, and three quasi-S (qS) velocities specify $A_{ii}(i = 4 : 6)$. The off-diagonal stiffness coefficients, however, are not individually related to the phase or group velocity along some particular directions. Next, we describe the relation between off-diagonal density normalized stiffness coefficients and group velocity.

Table 1. Body waves' velocities along the principal axes. Here V_{ij} $(i, j = 1, 2, 3)$ is the body wave velocity which propagates along the x_j-axis and polarized along the x_i-axis. For example V_{11} is the qP velocity propagating along the x_1-axis, and $V_{23}(= V_{32})$ is the qS velocity propagating along the x_3-axis and polarizing along the x_2-axis.

	Propagation		
Polarization	x_1	x_2	x_3
x_1	$V_{11} = \sqrt{A_{11}}$	$V_{12} = \sqrt{A_{66}}$	$V_{13} = \sqrt{A_{55}}$
x_2	$V_{21} = \sqrt{A_{66}}$	$V_{22} = \sqrt{A_{22}}$	$V_{23} = \sqrt{A_{44}}$
x_3	$V_{31} = \sqrt{A_{55}}$	$V_{32} = \sqrt{A_{44}}$	$V_{33} = \sqrt{A_{33}}$

Let $\vec{N} = (N_1, N_2, N_3) = (sin\Theta cos\Phi, sin\Theta sin\Phi, cos\Theta)$ be a unit vector in the direction of group velocity (ray direction), where Θ is the polar angle measured from the x_3-axis and Φ is the azimuthal angle measured from the x_1-axis. An approximate linearized expression for the qP group velocity (Song and Every, 2000; Daley and Krebes, 2006) in terms of orthorhombic A_{ij} is

$$\begin{aligned}\frac{1}{V^2(\vec{N})} \simeq\ & \frac{N_1^2}{A_{11}} + \frac{N_2^2}{A_{22}} + \frac{N_3^2}{A_{33}} - \\ & \frac{E_{23}N_2^2N_3^2}{A_{22}A_{33}} - \frac{E_{13}N_1^2N_3^2}{A_{11}A_{33}} - \frac{E_{12}N_1^2N_2^2}{A_{11}A_{22}}.\end{aligned} \tag{1}$$

where the quantities E_{ij}, are

$$\begin{aligned}E_{23} &= 2(A_{23} + 2A_{44}) - (A_{22} + A_{33}),\\ E_{13} &= 2(A_{13} + 2A_{55}) - (A_{11} + A_{33}),\\ E_{12} &= 2(A_{12} + 2A_{66}) - (A_{11} + A_{22}).\end{aligned} \tag{2}$$

The E_{ij} are called anellipsoidal deviation terms, as they describe the deviation of the wavefront from ellipsoidal anisotropy, see Appendix A. Equation 1 explicitly represents the qP group velocity in terms of the nine orthorhombic stiffness coefficients. Daley and Krebes (2006) derived equation 1 solving eikonal equation by the method of characteristics. Their orthorhombic qP group velocity formula is identical with that presented by Song and Every (2000) where the results were not established by rigorous derivation and were backed up by the numerical results.

The approximate qP group velocity, equation 1 is generally in good agreement with the exact calculations, even for highly anisotropic media. In Daley and Krebes (2006) the group velocity approximation was bench marked against the "exact" solution and found to be very accurate. In addition, it was compared to the approximation presented in Pšenčík and Farra (2005). The results were equivalent; about $0.2\% - 0.3\%$ deviation from exact traveltime calculations for weakly anisotropic media and 2% for a highly anisotropic (olivine) medium. Song and Every (2000) numerically validated equation 1, and showed that this formula can accurately account for the non-ellipticity of the qP group velocity surface in the absence of cusps.

Determination of stiffness coefficients

We determine the diagonal A_{ij} from direct measurements of qP- and qS-wave velocities, obtained from transmission traveltimes, along the x_1, x_2, and x_3-axes. To determine the off-diagonal stiffness coefficients, we use the qP group velocity expression, equation 1. It can be written as

$$D = BE_{23} + FE_{13} + LE_{12}, \tag{3}$$

where the coefficients D, B, F, L are defined as follows

$$\begin{aligned} D &= (\frac{{N_1}^2}{A_{11}} + \frac{{N_2}^2}{A_{22}} + \frac{{N_3}^2}{A_{33}}) - \frac{1}{{V(\vec{N})}^2}, \\ B &= \frac{{N_2}^2{N_3}^2}{A_{22}A_{33}}, F = \frac{{N_1}^2{N_3}^2}{A_{11}A_{33}}, L = \frac{{N_1}^2{N_2}^2}{A_{11}A_{22}}. \end{aligned} \tag{4}$$

Incorporating qP velocity measurements in m different directions, equation 3 can be used to write a linear system of m equations with three unknowns as

$$\begin{pmatrix} B_1 & F_1 & L_1 \\ \vdots & \vdots & \vdots \\ B_m & F_m & L_m \end{pmatrix} \begin{pmatrix} E_{23} \\ E_{13} \\ E_{12} \end{pmatrix} = \begin{pmatrix} D_1 \\ \vdots \\ D_m \end{pmatrix}, \tag{5}$$

or in a matrix form, $\mathbf{Ge} = \mathbf{d}$. We obtain the unknown vector $\mathbf{e} = (E_{23}, E_{13}, E_{12})$, vector of deviation terms, from a damped least-squares inversion, as $\mathbf{e} = (\mathbf{G}^T\mathbf{G} + \mu)^{-1}\mathbf{G}^T\mathbf{d}$ where μ is the damping factor. Knowing the deviation terms and diagonal A_{ij}, we determine the off-diagonal A_{ij} from equation 2 as

$$\begin{aligned} A_{23} &= (E_{23} - 4A_{44} + A_{22} + A_{33})/2, \\ A_{13} &= (E_{13} - 4A_{55} + A_{11} + A_{33})/2, \\ A_{12} &= (E_{12} - 4A_{66} + A_{11} + A_{22})/2. \end{aligned} \tag{6}$$

The accuracy of these estimations is dependent on the accuracy of the diagonal A_{ij}s.

NUMERICAL EXAMPLES

We test the validity of the proposed inversion for off-diagonal terms for two numerical examples. Using transmission traveltimes along various directions, generated from an anisotropic ray-tracing code, we calculate the group velocities. The first example, we use the A_{ij} of Greenhorn shale (Sayers and Ebrom, 1997), classified as weakly transversely isotropic. The stiffness coefficients for this model are $A_{11} = A_{22} = 19.19$, $A_{33} = 15.65$, $A_{13} = A_{23} = 7.06$, $A_{12} = 7.79$, $A_{44} = A_{55} = 4.11$, and $A_{66} = 5.7$ where all the A_{ij} have the units of (km/s)^2. The estimated value of A_{13} is to within 1.2% accurate. The second example is olivine, an orthorhombic medium with strong anisotropy. Its density normalized stiffness coefficients are $A_{11} = 9.779$, $A_{33} = 7.103$, $A_{13} = 2.163$, $A_{44} = 2.358$, and $A_{66} = 5.7$. Olivine's qP group velocity surface, in the (x_1, x_3) symmetry plane, is highly non-elliptical. In this case, our inversion for A_{13} resulted in a 2.3% error.

For the above weak and strong anisotropic examples, the proposed inversion for off-diagonal A_{ij}s are highly accurate. Of course, this accuracy is highly dependent on the accuracy of the independently estimated diagonal A_{ij}s, which in this case were assumed known without error.

PHYSICAL MODEL EXPERIMENT

The physical modeling system we used is designed to carry out simulated seismic surveys on scaled earth models, with a scale of $(1 : 10000)$ for length and time. This means that, for example, 1mm in the physical model represents 10m in real world. Having the same scale for length and time, the velocity of the medium remains unscaled.

We used flat-faced circular piezoelectric transducers, as both source and receiver, in acquiring transmission data; P- and S-transducers (Panametric V103 and V153) with diameter of 12.7 mm and a nominal central frequency of 300 kHz. These transducers convert electrical energy to mechanical energy and visa-versa, thus being capable of acting as either sources or receivers. As a receiver, the P- and S-transducers are sensitive to displacement normal and tangential to the contact face of the transducer, respectively, and represent vertical and horizontal component geophones. As a source, either P- or S-transducers generate both P- and S-waves, but the stronger generated P-wave emanating from the P-transducer and the stronger S-wave emanating from the S-transducer. Our modeling system is equipped with a robotic positioning system with the precision to within 0.1mm. We manually positioned the first source and receiver locations according to a predefined coordinate system; the nearest edge distance between the source and receiver defines the initial offset. Once the initial source-receiver offset is set, the subsequent increments in offset are computer controlled, thus are accurately known. There are separate arms for positioning the source and receiver. Vertical stacking of repeated source excitations for each receiver position and the progressive re-positioning of the receiver transducer generates a seismic gather. The source pulse is highly repeatable over many hours of acquisition. More details about the laboratory equipment and set-up are as described in Wong et al. (2009).

Our simulated fractured layer is made of LE-grade phenolic material, which is composed of laminated sheets of linen fabric bonded together with phenolic resin (Figure 2),

FIG. 2. Phenolic material from manufacturer.

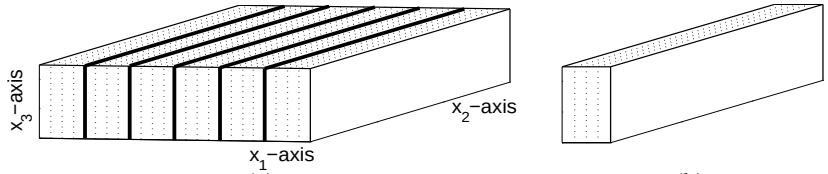

FIG. 3. (a) The simulated fractured medium in this study. (b) A slab of phenolic material with dashed lines displaying the linen planes.

with mass density of 1390 kg/m^3. Phenolic materials, because of their micro-layered texture, can be used to simulate finely layered structure rocks, such as sandstone, shale, or fractured limestone (Chang and Gardner, 1997). The phenolic material exhibits seismic anisotropy with apparent orthorhombic symmetry (Brown et al., 1991; Cheadle et al., 1991; Karayaka and Kurath, 1994). A manufactured board of phenolic material is milled to provide flat and perpendicular surfaces parallel to the the layering, the warp, and the weave of linen fabric as closely as possible. Hence, the symmetry of phenolic materials is relatively well controlled (Mah and Schmitt, 2001b). To construct our simulated fractured layer, a board of phenolic material with horizontally laid linen fabric was cut into slabs along planes orthogonal to the plane of linen layers. These were rotated 90° and bonded together under a uniform high pressure with epoxy. This constructed layer simulates a horizontal layer with vertical fractures of a single orientation. It has an approximate area of 57×57cm^2 and a thickness of 7cm (Figure 3).

Data acquisition

We acquire several 3-component (3C) transmission seismic data, over the simulated fractured layer. The vertical, radial, and transverse component data were acquired, utilizing P-transducers, radially polarized S-transducers, and transversely polarized S-transducers, as source and receivers, respectively. In our acquisition, the reference Cartesian coordinate system is chosen with respect to the simulated fractured layer symmetry system; the x_1-axis along slow direction, the x_2-axis along fast direction (isotropy plane), and the vertical x_3-axis along second fast direction. The transmission receiver lines were positioned along, 0°, 90°, 45°, 135° azimuth lines at the top surface (Figure 4(a-d)) with the source located at the bottom, and 0°, 90° azimuth lines at the top surface with the source also at the top with a distance from the receiver line (Figure 4(e-f)). The group velocity along different directions in the (x_1, x_3), (x_2, x_3), azimuth 45°, and azimuth 135° planes are read from the transmission profiles in Figure 4(a-d). The group velocity along different directions in the (x_1, x_2) plane are read from the profiles in Figure 4(e-f). Figure 5 shows the 3C data from one of our transmission shot gathers.

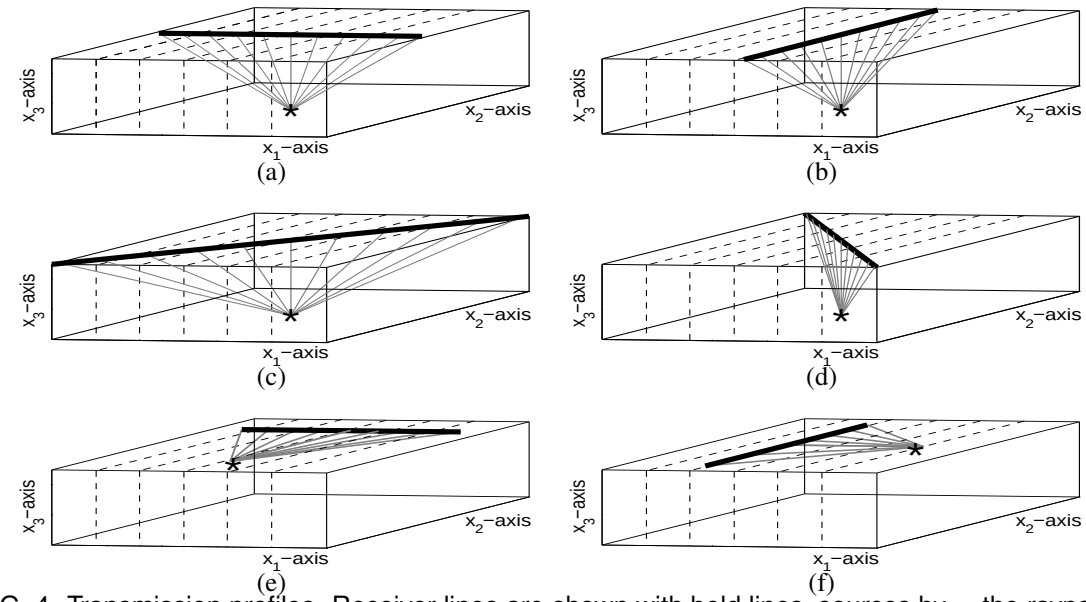

FIG. 4. Transmission profiles. Receiver lines are shown with bold lines, sources by $\star$, the raypaths connecting source-receivers with thin lines, slab joints with dash lines. (a-d) Receiver lines at top surface along 0°, 90°, 45°, and 135° (with respect to x_1-axis), with the source at bottom surface. (e-f) Receiver lines at top surface along 0°, and 90° with the source also at the top surface.

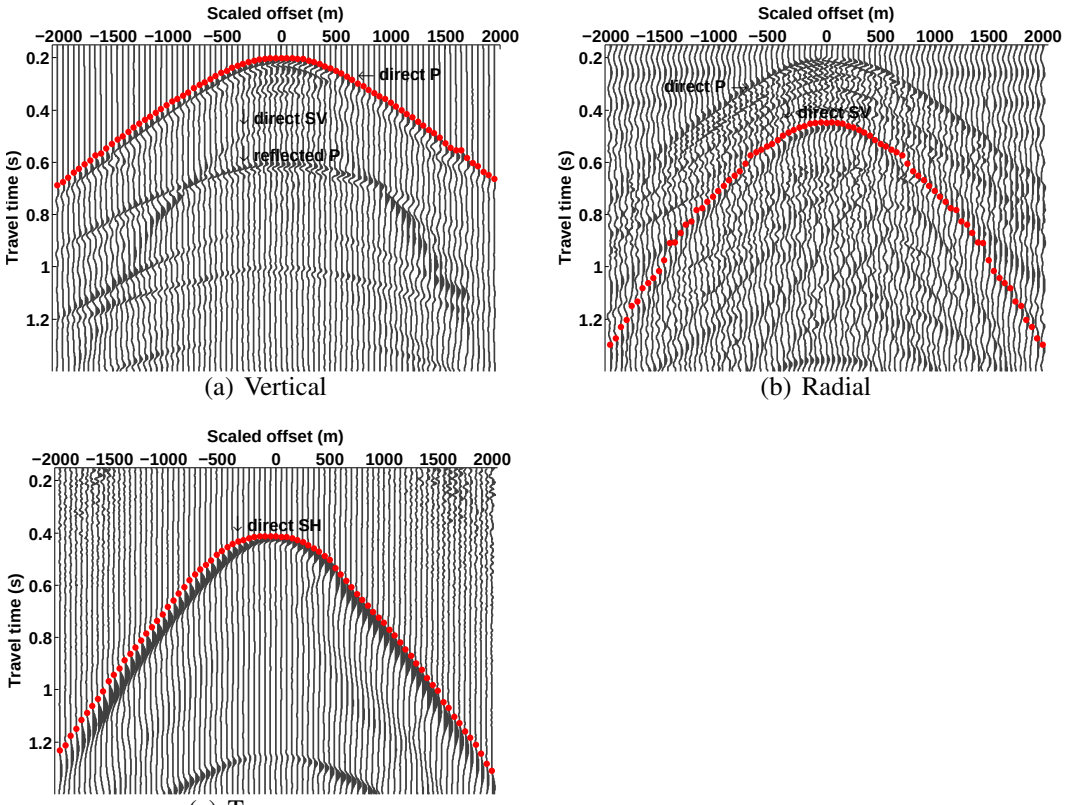

FIG. 5. The 3C transmission data acquired along the profile shown in Figure 4(a)). Red dots are first arrival picks of each mode. Displayed data have been filtered and a long-gate automatic gain control has been applied for the vertical and transverse components; the radial component data have been displayed with short window automatic gain control to boost the direct qS$_V$ arrival. The three components have similar noise levels.

Group velocity measurements

We treat our constructed simulated fractured layer as a homogeneous orthorhombic solid. For a transmission experiment, on a homogeneous layer, with point source and receiver transducers, the length of the straight line connecting the source and receiver divided by the first arrival traveltime yields the group velocity in the source-receiver raypath direction. For the transmission experiment, however, with the large source and receiver transducers, the effective source-receiver raypath is different from the source-receiver center-to-center distance. For our transmission experiment, on the homogeneous simulated fractured layer, with the transducers of the size 12.7mm, the effective source-receiver raypath is the straight line connecting the nearest edges of source and receiver transducers. Similar to Brown et al. (1991), we calculate the qP, qS-waves group velocities by dividing the effective source-receiver raypath to the first arrival traveltimes of each mode. The accurate transducer size is decided by recordings on an isotropic homogeneous plexiglas layer in advance. This edge-to-edge consideration for large transducer recordings is consistent with the traveltime data comparison in Sayers and Ebrom (1997) for data recorded by small (3.5mm in size) and large (12.7mm in size) transducers. Next provides a justification for considering the edge-to-edge distance as the raypath taken by the first arrival energy.

A circular physical model transducer approximates a circular seismic array. In Figure 1, we display a seismic wavefront radiated and detected by source and receiver arrays, using finite-difference medeling. Plane waves are generated in the direction normal to the face of source transducer element. The first arrival recorded at the receiver, is generated by the closest source and receiver points of the array. The first arrival energy, hence, has traveled the Euclidian distance between the nearest edges of the transducers.

The qP group velocities, of the simulated fractured medium, are determined from qP first arrival traveltimes picked on the vertical component data. The qS_V and qS_H group velocities are obtained from qS-waves first arrivals picked on the radial and transverse data components. The qP and qS_H first arrivals are strong and easy to pick. The qS_V first arrivals, however, are difficult to be accurately picked (Figure 5). At this point, we suspect that this is due to presence of cusp for qS-wave. The picks for middle range angles are ambiguous.

Table 2. Phenolic qP- and qS-velocity in principal directions.

Velocity (m/s)	Pulse measurements	Seismic measurements
V_{11}	2926 ± 74	2950 ± 70
V_{22}	3542 ± 77	3560 ± 70
V_{33}	3425 ± 80	3500 ± 70
V_{23}	1670 ± 20	1700 ± 35
V_{13}	1525 ± 10	1530 ± 35
V_{12}	1500 ± 15	1510 ± 35

To check the accuracy of the group velocities from physical model transmission first arrival traveltimes, we compared the qP and qS velocities along the previously defined (x_1, x_2, x_3) axes to an average of the measured velocities from a conventional direct pulse

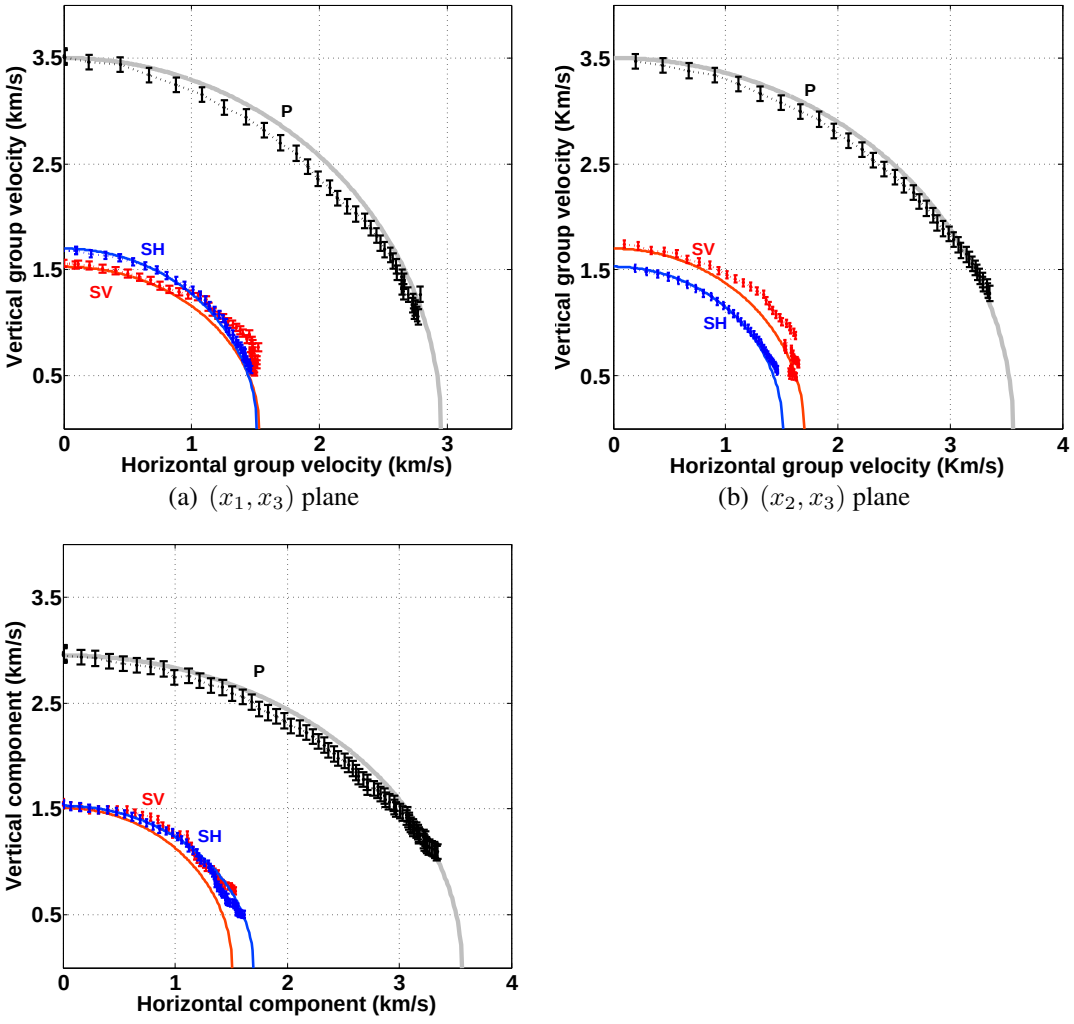

(a) (x_1, x_3) plane

(b) (x_2, x_3) plane

(c) (x_1, x_2) plane

FIG. 6. The group velocity surfaces for the three modes (qP, qS$_V$, qS$_H$) in the three symmetry planes. An elliptical wavefront is plotted for comparison in solid. The measured velocities in the $0°$ and $90°$ directions, are considered as the major and minor axes of the ellipse. Group angles are plotted with respect to the vertical axis for the (x_1, x_3) and (x_2, x_3) planes, and with the x_2-axis for the (x_1, x_2) plane.

measurement conducted on 18 individual phenolic slabs (Table 2), similar to those used in constructing our simulated fractured layer. Table 2 shows these comparisons. We find that the group velocities from physical model transmission data are well estimated. We considered the errors of ± 70m/s and ± 35m/s for the qP- and qS-velocities measured from from physical model data, using 0.1mm error in distance and 0.004s error for first arrival time picks ($1/8$ of the dominant wavelength). The statistical errors of the velocities measured from pulse measurements are calculated from the standard deviation of the values.

The qP and qS group velocity surfaces, polar plots of group velocity versus propagation angle, for the symmetry planes are shown in Figure 6. The qS$_H$ wavefronts are purely ellipsoidal, the qP wavefronts deviate slightly from the ellipsoidal, and the qS$_V$ wavefronts deviate significantly from the ellipsoidal.

SIMULATED FRACTURED LAYER A_{IJ}

We present the estimated A_{ij} of the simulated fractured layer, and their statistical uncertainties, listed in Table 3; the statistical uncertainties are estimated by introducing a small perturbation, representing uncertainty, in the measured group velocities and observing the corresponding changes in the stiffness coefficients.

Table 3. Density-normalized stiffness coefficients of the simulated fractured layer. The A_{ij} have the units of (km/s)^2.

8.70 ± 0.41	4.9 ± 0.21	4.96 ± 0.21	0	0	0
	12.67 ± 0.49	5.58 ± 0.23	0	0	0
		12.25 ± 0.49	0	0	0
			2.89 ± 0.12	0	0
				2.34 ± 0.11	0
					2.28 ± 0.11

As an accuracy test for the estimated stiffness coefficients, we calculate the group velocities predicted by these estimations. We first calculate the theoretical exact phase velocities followed by the exact group velocities; the exact explicit orthorhombic phase velocity expression is given by Tsvankin (2001), and the expression relating the phase and group velocities are employed (Appendix B). For the symmetry plane, Figure 7 compares the measured group velocities from transmission data and calculated theoretical velocities. The theoretical velocities match the measured velocities reasonably well. There are, however, some discrepancies between the theoretical group velocities and measured group velocities. The maximum discrepancies are 140m/s for qP and 100m/s and 40m/s for qS$_V$ and qS$_H$ velocities. These small discrepancies could be due to our assumption of homogeneity for the simulated fractured layer, the employment of the approximate orthorhombic group velocity expression rather than an exact form, or the assumption of orthorhombic symmetry for the simulated fractured layer. A lower symmetry assumption such as monoclinic might be more indicative of the simulated fractured layer.

The stiffness coefficients of the simulated fractured layer characterize the anisotropy of the medium, while the strengths of anisotropy are hidden. The dimensionless orthorhombic anisotropic parameters are defined in Tsvankin (1997), which express the measure of anisotropy similar to the well-known Thomsen (1986) coefficients ϵ, δ, and γ for VTI media. Using expressions the orthorhombic parameters in terms of the stiffness coefficients are given in Table 4. These parameters of the stimulated fractured layer and their statistical uncertainties are as follows:

$$\begin{aligned}
&\delta^{(2)} = -0.185 \pm 0.002, && \delta^{(1)} = -0.069 \pm 0.001, && \delta^{(3)} = 0.228 \pm 0.004,\\
&\epsilon^{(2)} = -0.145 \pm 0.003, && \epsilon^{(1)} = 0.017 \pm 0.0003, && V_{P0} = 3500 \pm 70 \text{ m/s}\\
&\gamma^{(2)} = -0.106 \pm 0.002, && \gamma^{(1)} = -0.013 \pm 0.0003, && V_{S0} = 1700 \pm 35 \text{ m/s}
\end{aligned}$$

The stiffness coefficients of the simulated fractured layer given in Table 3, reveal that the experimental layer approximates a HTI medium with x_1 being the symmetry axis and

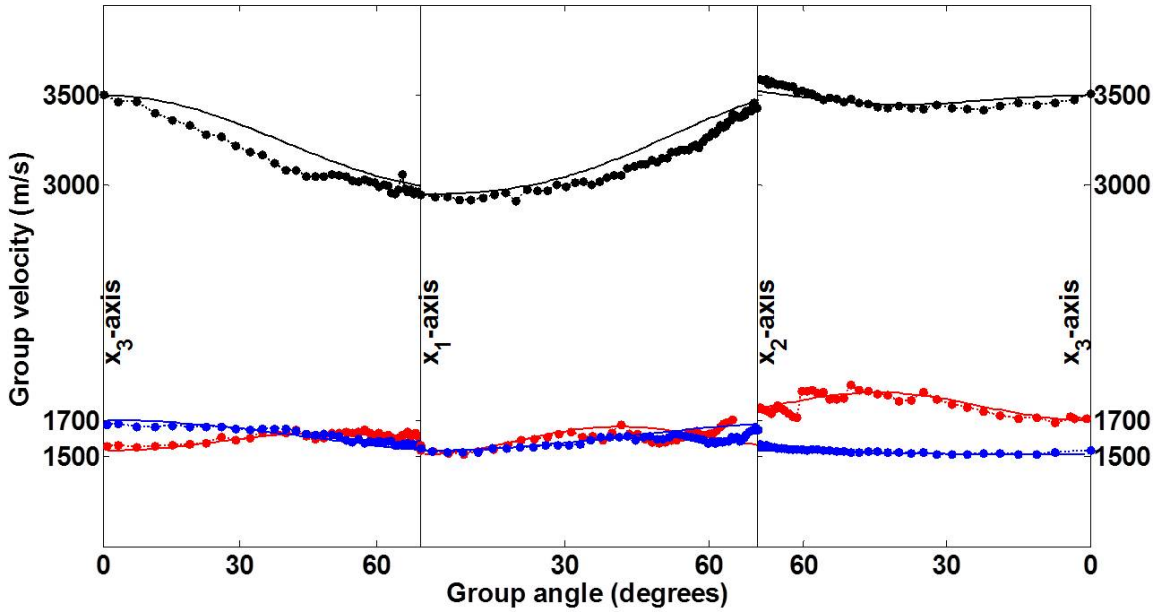

FIG. 7. The group velocities versus propagation angle in the symmetry planes (x_1, x_3), (x_2, x_3) and (x_1, x_2). The solid lines are theoretical velocities and the dotted lines are measured ones. The qP velocities are shown in black, qS_V in red, and qS_H in blue.

the (x_2, x_3) plane is the isotropic plane. If we treat the simulated fractured layer as a HTI medium with x_1-axis as the symmetry axis, the five effective HTI anisotropic parameters required in investigating the azimuthally AVO responses of the medium $(\alpha, \beta, \epsilon^{(V)}, \delta^{(V)}, \gamma)$, used by Rüger (2001), are

$$\begin{aligned} \alpha &= V_{P0} = 3500 \text{ m/s}, \\ \beta &= V_{S0} = 1700 \text{ m/s}, \\ \delta^{(V)} &= \delta^{(2)} = -0.185, \\ \epsilon^{(V)} &= \epsilon^{(2)} = -0.145, \\ \gamma &= \frac{A_{44} - A_{55}}{2A_{55}} = 0.117. \end{aligned}$$

Converting these HTI parameters to their equivalent Thomsen (1986) coefficients ϵ, δ, and γ which carry the conventional meaning of anisotropy, the fractional differences of the fast and slow velocities, results in the following values: $\epsilon = 0.204, \gamma = 0.117$, and $\delta = 0.116$. These values indicate the weak anisotropy for our simulated fracture layer.

Table 4. Tsvankin (1997) orthorhombic parameter relations to the stiffness coefficients.

$\delta^{(2)} = \frac{(A_{13}+A_{55})^2-(A_{33}-A_{55})^2}{2A_{33}(A_{33}-A_{55})}$	$\delta^{(1)} = \frac{(A_{23}+A_{44})^2-(A_{33}-A_{44})^2}{2A_{33}(A_{33}-A_{44})}$	$\delta^{(3)} = \frac{(A_{12}+A_{66})^2-(A_{11}-A_{66})^2}{2A_{11}(A_{11}-A_{66})}$
$\epsilon^{(2)} = \frac{A_{11}-A_{33}}{2A_{33}}$	$\epsilon^{(1)} = \frac{A_{22}-A_{33}}{2A_{33}}$	$V_{P0} = \sqrt{A_{33}}$
$\gamma^{(2)} = \frac{A_{66}-A_{44}}{2A_{44}}$	$\gamma^{(1)} = \frac{A_{66}-A_{55}}{2A_{55}}$	$V_{S0} = \sqrt{A_{55}}$

CONCLUSIONS AND DISCUSSION

We have presented a straightforward method to characterize an orthorhombic material and suggested the use of group-velocity measurements to estimate the stiffness coefficients. We obtained the group velocity in various directions by measuring direct-arrival traveltimes on physically modeled 3C transmission gathers. The effect of relatively large physical model transducers were mitigated by using a single geometric correction. Our method is based on a relatively new approximate relationship between group velocity and orthorhombic stiffness coefficients. The orthorhombic qP velocity expression by Song and Every (2000) and Daley and Krebes (2006) results in off-diagonal stiffness coefficients estimates. We showed that the estimates of stiffness coefficients, for our physical layer, are consistent with our velocity data, by comparing the measured velocities with the calculated theoretical velocities predicted by the estimated stiffness coefficients. Our experimental physical layer approximates a weakly anisotropic HTI layer, or equivalently a vertically fractured transversely isotropic layer.

The characterization of physical models are usually by employing the phase velocities, as the theoretical link between stiffness coefficients and phase velocities are well understood. Measurement of phase velocities, however, are cumbersome. The group velocity measurements are near-to-exact and straightforward but comparable theoretical linkage for group velocities and stiffness coefficients are not. We draw the readers attention to the practicality of the linear orthorhombic group velocity expression that was used. A qP group velocity approximation in a general 21-parameter weakly anisotropic medium is presented in Daley and Krebes (2007). This could be employed in characterization of media with less symmetry. An approximation for orthorhombic qS-wave is also available (Song and Every, 2000).

We assume homogeneity for our simulated fractured medium and believe that the frequency dispersion in this experimental layer in minimal. The observed changes in the wavelet, in our transmission data, are mostly the effect of transducer size. We numerically modeled a P-wave shot gather, over an isotropic homogenous model with the dimensions of our simulated fractured layer, using finite difference modeling with the source and receiver array length equal to our transducer's size. The gather is shown in Figure 8. This modeling indicates the apparent change in wavelet shape from near to far offset is due mostly to the large size of the source and receiver transducers and not due to frequency or grid dispersion.

ACKNOWLEDGMENTS

We thank the sponsors of CREWES for their financial support. This work is also supported by NSERC, the National Sciences and Engineering Research Council of Canada. Eric Gallant's work in constructing the phenolic model is most appreciated.

APPENDIX A
Anellipsoidal deviation terms

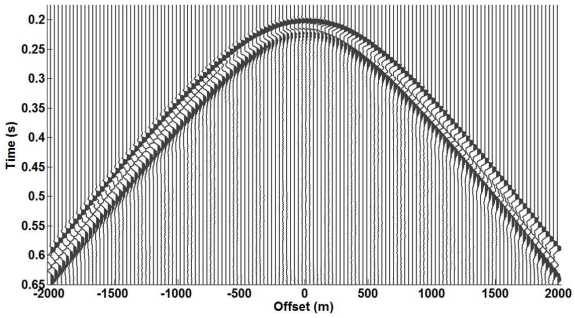

FIG. 8. P-wave shot gather generated by acoustic finite-difference modeling with the source and receiver sizes equivalent to the physical model experiment.

This appendix provides the basis on how the E_{ij} terms in theory section can be interpreted as deviation, from elliptical anisotropy terms. We start with the definition of a velocity surface, plotting the phase/group velocity of a given mode (qP-, qS-waves) as the radius-vector in all directions. The group velocity surface, therefore, is the wavefront at unit time. An orthorhombic medium has ellipsoidal anisotropy, if the wavefront, and hence the group velocity surface, is an ellipsoid, then, the formula for group velocity surface is that of an ellipsoid. The qP ellipsoidal group velocity surface, then, has the exact form

$$\frac{1}{V^2(\vec{N})} = \frac{N_1^2}{A_{11}} + \frac{N_2^2}{A_{22}} + \frac{N_3^2}{A_{33}}, \tag{7}$$

and the corresponding phase velocity has the form (Musgrave (1970), equations 8.2.1 and 8.2.2b page 96)

$$v^2(\vec{n}) = A_{11}n_1^2 + A_{22}n_2^2 + A_{33}n_3^2, \tag{8}$$

where $\vec{n} = (n_1, n_2, n_3) = (sin\theta cos\phi, sin\theta sin\phi, cos\theta)$ is the unit vector normal to the wavefront, with θ and ϕ having similar definitions as Θ and Φ.

For a general weakly anisotropic medium, the first-order linearized approximation for qP phase velocity is $\rho v^2(\vec{n}) \simeq c_{ijkl}n_in_jn_kn_l$, (Backus, 1965). Defining density normalized stiffness tensor as $a_{ijkl} = c_{ijkl}/\rho$, it reads

$$v^2(\vec{n}) \simeq a_{ijkl}n_in_jn_kn_l. \tag{9}$$

Using Voigt notation for indexes $(11 \to 1, 22 \to 2, 33 \to 3, 23 \to 4, 13 \to 5, 12 \to 6)$, the density-normalized stiffness coefficients A_{ij} will be obtained as $a_{ijkl} = A_{mn}$. Expanding equation 9 for orthorhombic symmetry one obtains

$$\begin{aligned} v^2(\vec{n}) \quad \simeq \quad & A_{11}n_1^4 + A_{22}n_2^4 + A_{33}n_3^4 + 2(A_{12} + 2A_{66})n_1^2n_2^2 + \\ & 2(A_{13} + 2A_{55})n_1^2n_3^2 + 2(A_{23} + 2A_{44})n_2^2n_3^2. \end{aligned} \tag{10}$$

Equation 10 can be modified to read (Daley and Krebes, 2006),

$$\begin{aligned} v^2(\vec{n}) \quad \simeq \quad & A_{11}n_1^2 + A_{22}n_2^2 + A_{33}n_3^2 + \\ & E_{23}n_2^2n_3^2 + E_{13}n_1^2n_3^2 + E_{12}n_1^2n_2^2. \end{aligned} \tag{11}$$

where the quantities E_{ij} were perviously defined. Equation 11 is an expression for orthorhombic phase velocity in an approximate form. Comparing it with the ellipsoidal phase

velocity (equation 8), we interpret the E_{ij} as anellipsoidal deviation terms. Helbig (1983) states, that in the study of transverse isotropy by Rudzki (1911), the wavefront for the compressional wave in the (x_1, x_3) plane is ellipsoidal if and only if $(A_{11} - A_{55})(A_{33} - A_{55}) - (A_{13} + A_{55})^2 = 0$. The E_{13} deviation term in equation 2 is a linearized approximation of this deviation term used by Rudzki (1911).

APPENDIX B
Exact orthorhombic velocity expressions

Tsvankin (1997) presented the exact orthorhombic phase velocity expressions for the symmetry planes. For propagation in the (x_1, x_3) symmetry plane, the exact qS$_H$ phase velocity is

$$v_{S_H}(\theta)^2 = A_{66}\sin^2\theta + A_{44}\cos^2\theta, \tag{12}$$

where θ is the phase angle with the x_3-axis. The exact phase velocity of the qP and qS$_V$ modes are

$$\begin{aligned} 2v^2(\theta) &= (A_{11}+A_{55})\sin^2\theta + (A_{33}+A_{55})\cos^2\theta \\ &\pm \sqrt{\left[(A_{11}-A_{55})\sin^2\theta - (A_{33}-A_{55})\cos^2\theta\right]^2 + 4(A_{13}+A_{55})^2\sin^2\theta\cos^2\theta}, \end{aligned} \tag{13}$$

where the plus and minus signs correspond to the qP and qS$_V$ modes of propagation, respectively. For the propagation in other symmetry planes, the appropriate indexes are used.

For the orthorhombic symmetry planes, the group velocity and group angle, of three wave modes, are related to the phase velocity by (Berryman, 1979)

$$V_G = v(\theta)\sqrt{1 + \left(\frac{1}{v(\theta)}\frac{dv(\theta)}{d\theta}\right)}, \tag{14}$$

$$\tan\psi = \frac{\tan\theta + \frac{1}{v(\theta)}\frac{dv(\theta)}{d\theta}}{1 - \frac{\tan\theta}{v(\theta)}\frac{dv(\theta)}{d\theta}}, \tag{15}$$

where V_G is the magnitude of the group angle, ψ is the group angle, v is phase velocity, and θ is the phase angle.

REFERENCES

Backus, G. E., 1965, Possible forms of seismic anisotropy of the uppermost mantle under oceans: Journal of Geophysical Research, **70**, No. 14, 3429.

Berryman, J. G., 1979, Long-wave elastic anisotropy in transversely isotropic media: Geophysics, **44**, No. 5, 896–917.

Brown, R. J., Lawton, D. C., and Cheadle, S. P., 1991, Scaled physical modeling of anisotropic wave propagation: multioffset profiles over an orthorhombic medium: Geophysical Journal International, **107**, No. 3, 693–702.

Chang, C., and Gardner, G. H. F., 1997, Effects of vertically alighned subsurface fractured on seismic reflections: A physical model study: Geophysics, **62**, 245–252.

Cheadle, S. P., Brown, R. J., and Lawton, D. C., 1991, Orthorhombic anisotropy:a physical seismic modeling study: Geophysics, **56**, No. 10, 1603–1613.

Daley, P. F., and Krebes, E. S., 2006, Quasi- compressional group velocity approximation in a weakly anisotropic orthorhombic medium: Journal of Seismic Exploration, **14**, 319–334.

Daley, P. F., and Krebes, E. S., 2007, Quasi-compressinal group velocity approximation in a general 21-parameter weakly anisotropy medium: Journal of Seismic Exploaration, **16**, 41–55.

Dellinger, J., and Vernik, L., 1994, Do traveltimes in pulse-transmission experiments yield anisotropic group or phase velocities?: Geophysics, **59**, No. 11, 1774–1779.

Every, A. G., and Sachse, W., 1992, Sensitivity of inversion algorithms for recovering elastic constants of anisotropic solids from longitudinal wavespeed data: Ultrasonics, **30**, No. 1, 43–48.

Helbig, K., 1983, Elliptical anisotropy-its significant and meaning: Geophysics, **48**.

Karayaka, M., and Kurath, P., 1994, Deformation and faliure behavior of woven composite laminates: J. Eng. Mat and Technol., **116**, 222–232.

Kebaili, A., and Schmitt, D. R., 1997, Ultrasonic anisotropic phase velocity determination with radon transformation: Journal of the Acoustical Society of America, **101**, 3278–3286.

Kim, K. Y., Sribar, R., and Sachse, W., 1995, Analytical and optimization procedures for determination of all elastic constants of anisotropic solids from group velocity data measured in symmetry planes: Journal Appl. Phys., **77**, No. 11, 5589–5600.

Mah, M., and Schmitt, D. R., 2001a, Experimental determination of the elastic coefficients of an orthorhombic material: Geophysics, **66**, 1217–1225.

Mah, M., and Schmitt, D. R., 2001b, Near point-source longitudinal and transverse mode ultrasonic arrays for material characterization: IEEE, **48**, 691–698.

Musgrave, M. J. P., 1970, Crystal Acoustics: Holden-Day, San Francisco.

Pšenčík, I., and Farra, V., 2005, First-order ray tracing for qp wave in inhomogeneous weakly anisotropic media: Geophysics, **70**, D65–D75.

Rudzki, M. P., 1911, Parametrische darstellungd er elastischen welle in anisotropen medien: Anzeiger der Akademie der Wissenachaften Krakau, 503–536.

Rüger, A., 2001, Reflection coefficients and azimuthal avo analysis in anisotropic media: Goephysical Monograph Series.

Sayers, C. M., and Ebrom, D., 1997, Seismic traveltime analysis for azimuthally anisotropic media: Theory and experiment: Geophysics, **62**, No. 5, 1570–1582.

Song, L. P., and Every, A. G., 2000, Approximate formulae for acoustic wave group slownesses in weakly orthorhombic media: Journal of Physics D: Applied Physics, **33**, L81–L85.

Thomsen, L., 1986, Weak elastic anisotropy: Geophysics, **51**, No. 10, 1954–1966.

Tsvankin, I., 1997, Anisotropic parameters and p-wave velocity for orthorhombic media: Geophysics, **62**, No. 4, 1292–1309.

Tsvankin, I., 2001, Seismic signatures and analysis of reflection coefficients in anisotropic media: Elsevier, Amsterdam.

van der Baan, M., 2002, Estimating anisotropy parameters and traveltimes in the $\tau - p$ domain: Geophysics, **67**, 1076–1086.

Vestrum, R. W., 1994, Group- and phase-velocity inversions for the general anisotropic stiffness tensor: M.Sc. Thesis, University of Calgary.

Wong, J., Hall, K. W., Gallant, E. V., Maier, R., Bertram, M., and Lawton, D. C., 2009, Seismic physical modeling at university of calgary: CSEG Recorder.